

Method for three-dimensional visualization of neurodegeneration in cupric-silver stained serial rat brain slices

Leonid Bunegin
Gleb P. Tolstykh
Jerry F. Gelineau

University of Texas Health Science Center
at San Antonio
Department of Anesthesiology
7703 Floyd Curl Drive
San Antonio, Texas 78229-3900
E-mail: bunegin@uthscsa.edu

Abstract. The spatial distribution of neurodegeneration in brains is difficult to visualize when working from 2-D serial slices. In studies where repetitive operant behavior measurements are made over several weeks following organic solvent exposure, definitive evidence of degeneration in brain structures may have been significantly cleared by the time the tissue is prepared histologically. The only remaining evidence that injury has occurred may be nothing more than neuronal and cellular debris. By choosing stains that are specific for this type of residual and/or indicative of specific pathology, a 3-D representation of the spatial distribution of the neuronal and cellular debris fields within the organ can be highlighted and displayed. We present a method for visualizing the spatial distribution of neuronal degeneration that can result from low-level organic solvent exposure scenarios. A cupric-silver stain highly specific for neuronal degeneration is used to identify neuronal debris fields in 73 serial slices of brains of rodents that were exposed to toluene vapors. Serial brain sections stained with cupric-silver are scanned at 600 dpi using a gray-scale protocol. Using commercially available software, scans are assembled into 3-D images showing both topographical and internal anatomical details. The reassembled images are further processed into stereo pairs. Gray-scale scans are compared to the original sections to establish gray-scale ranges for healthy and damaged tissue and artifact staining. © 2005 Society of Photo-Optical Instrumentation Engineers. [DOI: 10.1117/1.1896006]

Keywords: three-dimensional; neurodegeneration; toluene; cupric-silver stain; rat; brain; histopathology.

Paper 03095 received Jul. 15, 2003; revised manuscript received Feb. 2, 2004; accepted for publication Sep. 8, 2004; published online Apr. 14, 2005.

1 Introduction

The analysis of stained histopathologic serial tissue sections continues to be a laborious, time-consuming process of microscopic examination and preparation of a detailed record of the visual observations. This approach makes it difficult to project spatial relationships between tissue structures and injury or degeneration of the tissue. Rating schemes that identify the extent of damage are often subjective, and provide little basis for statistical analysis. Alternative approaches such as projection of individual sections onto paper followed by tracing, planimetry, segment volume calculation, and summation to obtain volume estimates of regions of interest can be equally time consuming and suffer from a high degree of bias and imprecision. Computer software designed to identify regions of interest in 2-D images shorten analysis time but still do not provide direct visualization of the spatial distribution of the observed pathology. Analysis can be further complicated when attempting to correlate subtle changes in operant performance following low-level solvent exposure and histologic

changes such as neuronal degeneration. Since operant behavior testing can require several weeks, definitive indications of degeneration can be substantially cleared, leaving behind little more than debris fields in the affected areas.

Recent advances in image analysis software have facilitated the development of three-dimensional (3-D) reconstructive imaging methodologies from sequential serial tissue sections. The primary focus of these methodologies has been the modeling of anatomical structures such as glomerular capillaries, skeletal muscle, cytoplasmic interdigitation of cellular structures, and coronary microvasculature.¹⁻⁴ However, serial sections of histologically stained tissue can also be assembled into a 3-D representation of the original tissue. Appropriately chosen stains that are specific to a particular pathology or anatomical structure can be used to highlight the region of interest. A 3-D representation of the areas of interest and their spatial distribution within the organ can then be displayed. Since the 3-D reconstructions are built up from volume elements (voxels), reasonably accurate estimates of volume can be made for several regions of interest simultaneously.

Address all correspondence to Professor Leonid Bunegin, University of Texas Health Science Center, Department of Anesthesiology, 7703 Floyd Curl Drive, San Antonio, Texas 78229-3900.

Image analysis systems capable of 3-D assembly are generally composed of expensive acquisition hardware and analysis software. This paper describes a method for visualizing the spatial distribution of histopathology within tissue based on 3-D reconstruction of stained serial histology sections utilizing computer systems generally available in most laboratories. In addition, quantification of the extent of degeneration is also described. The method entails histologic preparation of sequential serial slices of brain tissue by specific staining then scanning, capturing, and processing the images followed by volume rendering using VoxBlast™ (VayTek, Fairfield, Iowa).

2 Materials and Methods

2.1 Subjects

The protocols used in this study were reviewed and approved by the Institutional Animal Care and Use Committee. Sixteen male and 16 female Sprague Dawley rats were obtained from Charles River Laboratories (Wilmington, Massachusetts). The rodents were between 54 and 58 days old and weighed 180 to 200 g when received. Animals were individually housed in polycarbonate cages with bedding of hardwood shavings. Caloric regulation maintained animal weight between 75 and 80% of the age-adjusted free-feeding weight based on growth curves supplied by the vendor. Water was available *ad libitum* from water bottles located in the cages.

2.2 Experimental Design

Four exposure groups with eight subjects (four female and four male) each were used. Rats were exposed to either a single high dose of toluene (acute, 1600 ppm×6 h=9600 ppm/h) or to a repeated low dose of toluene (repeat, 80 ppm×6 h×20 day=9600 ppm/h). Two control groups were similarly exposed to clean air only. After a 2-week period with no further exposure, both groups (acute and repeat) and one control group (trigger control) were exposed to 10 ppm toluene for 1 h daily for 2 weeks while the remaining control group (clean control) was exposed to clean air for 1 h daily for 2 weeks.

2.3 Exposure Chamber

Rodents were exposed to the test environment by whole body inhalation. Certified ACS (99.9% pure) toluene (CAS Number 108-88-3) obtained from Fisher Scientific (Hampton, New Hampshire) was used for toluene exposure. The exposure chambers were 1.5 m³ and constructed of stainless steel and glass. The flow rate through the chambers was adjusted so that 12 to 15 conditioned, high-efficiency particulate air (HEPA)-filtered air changes occurred every hour. Chamber flow and temperature were computer monitored continuously during the exposure periods. Audible alarms were triggered if chamber flow deviated by 5% of the programmed values or when temperature fell below 64 or above 79°F.

Toluene vapors were introduced into a conditioned air stream that flowed through a computer-controlled in-line heated evaporator unit. The physical characteristics of toluene were programmed into the system, enabling the computer to control delivery of toluene to the evaporator via peristaltic pump based on air temperature and flow to generate the desired toluene vapor concentration. Chamber toluene concentrations were monitored at 3-min intervals using a dedicated

gas chromatography system (MTI M200D™, Fremont, California). The system alerted the operator if toluene concentrations deviated from programmed set points. The set points for the 10-ppm exposure were 9 and 11 ppm; for 80 ppm, they were 75 and 85 ppm; and for 1600 ppm, they were 1400 and 1800 ppm. Toluene concentrations reached target levels within 15 min of toluene initiation, and fell to near zero within 15 min of turning off the toluene supply.

2.4 Exposure Procedures

Exposures were carried out for 6 h/day, Monday through Friday, for four consecutive weeks. The repeat group was placed into a chamber and exposed to 80 ppm of toluene for 20 days. The acute, trigger control, and clean control groups were placed into another chamber and exposed to clean air only for 19 days. On the 20th day, the acute group was placed into a third chamber and exposed to 1600 ppm while the control groups continued to be exposed to clean air only. Animals were then given a 16-day “rest” period. During the next 23 successive weekdays beginning on a Monday, daily 1-h, 10-ppm toluene exposures were given to the repeat, acute, and trigger control groups. The clean control was similarly exposed but to clean air only.

2.5 Staining Procedure

Following the completion of the exposure scenario, the rats were anesthetized with a 50-mg/kg dose of sodium pentobarbital injected intraperitoneally, then intracardially perfused with buffered (pH 7.4) phosphate wash to remove all blood from the brain. A solution of 10% paraformaldehyde buffered (pH 7.2) with sodium cacodylate was then infused so as to fix the brain tissue. Brains were removed from the cranium, and all 16 brains were embedded as a 4×4 block in a gelatin matrix at NeuroScience Associates using MultiBrain Technology™ (Knoxville, Tennessee). The block of embedded brains was allowed to cure then rapidly frozen by immersion in isopentane chilled to -70°C with dry ice. The block was mounted on the freezing stage of a sliding microtome and sectioned coronally at a 40-μm thickness, beginning at the spinal medullary junction and proceeding to the olfactory bulbs. All sections were collected sequentially into containers containing 4% paraformaldehyde buffer with sodium cacodylate (pH 7.2).

A sequential set of every eighth section (at 360-μm intervals) was selected for staining. An amino cupric silver stain, highly specific for degenerating neurons, was used to identify neuronal degeneration in 73 serial sections in each of the eight brains in each group. The amino cupric staining followed the protocol described by deOlmos et al.⁵ The stained sections containing the 4×4 matrix of coronal slices were mounted on glass slides and counter stained with Neutral Red to reveal cell bodies.

2.6 Image Capture

The glass slides were scanned on a flat bed scanner (UMAX Astra 1200S™, Fremont, California) at 600 dpi in the reflective mode using a gray-scale protocol (Fig. 1). The default scanner settings were used for all scans. The gray-scale maps of the images were not modified during postprocessing. Adobe Photoshop 4.0™ (Adobe Systems, San Jose, Califor-

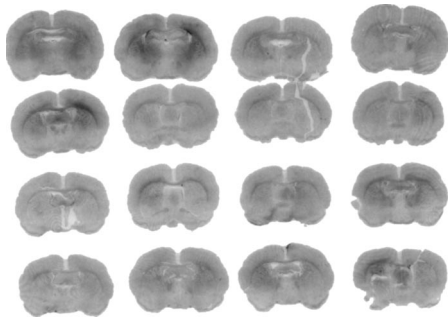


Fig. 1 Gray-scale scan of the 39th Cu-Ag stained coronal section of toluene-exposed rat brains.

nia) was used to extract individual sections to a 380×250-pixel canvas, and saved as 8-bit tagged image file format (TIFF) files. Since Photoshop™ automatically pastes the extracted images onto the center of the new canvas, only manual rotational adjustment was used to achieve final alignment. The aligned images were stacked and rendered into a three dimensional image using VoxBlast™ (VayTek, Fairfield, Iowa). The single volume rendering feature was used to produce 3-D surface images of the reconstructed brains. The maximum intensity rendering feature was used to generate transparent 3-D images highlighting the stained internal structures that represented the debris fields. The software simultaneously generated a histogram of the voxel gray-scale distribution.

Several cupric-silver-stained sections were randomly selected from each experimental animal and examined under light microscopy to visualize degenerated neuronal structures. The corresponding gray-scale image of the section was located and opened into PhotoShop™ for inspection and identification of the matching structures. The eyedropper function in PhotoShop™ was positioned over each structure and the gray-scale value recorded from the image information window. The gray-scale shades associated with neuronal debris ranged between 110 and 140 with artifact typically falling below 50. Voxels exhibiting gray-scale shades between 110 and 140 were summed then multiplied by the voxel volume to determine the volume of the neuronal debris field. Data sets were re-rendered in the maximum intensity mode with transparency adjustment so as to highlight the debris fields and create see-through 3-D images. Scans were further processed into stereo pairs.

2.7 Statistical Analysis

Data are presented as means±standard deviations. Mean brain and neuronal debris field volumes were compared using a single-factor analysis of variance of repeated measures followed by a Student-Neuman-Keuls posttest were indicated. Rejection of the null hypothesis was set at $p < 0.05$.

3 Results

Scanning the stained slides at 600 dpi resulted in an image resolution of 236.2 pixels/cm with a pixel dimension of 0.042 × 0.042 mm. Voxel volume was calculated by multiplying the pixel area by the interslice interval (0.36 mm), resulting in a voxel volume of $6.35 \times 10^{-4} \text{ mm}^3$.

Figure 2 shows 3-D stereo pairs of the surface and see-

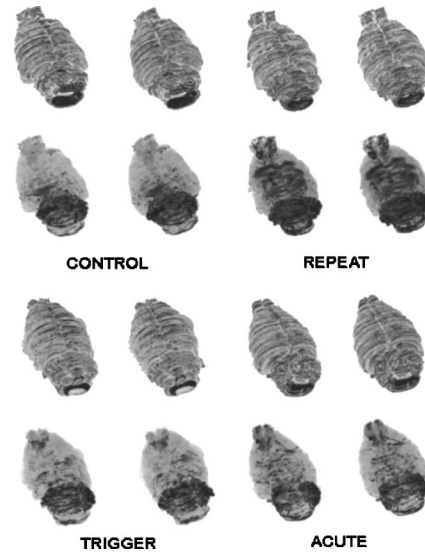


Fig. 2 Stereo pairs depict reassembly of individual brain slices (upper) and internal Cu-Ag stain distribution (lower) resulting from each exposure condition.

through images of a representative brain from each exposure group. A greater level of staining appears in the forceps minor corpus callosum, caudate putaman, corpus callosum, elements of the hippocampus, and the cerebellar lobules of the repeat exposure group relative to the clean control group. Both the acute and trigger control groups also show increased diffuse staining compared to the control group but to a lesser extent than the repeat group.

The voxel gray-scale distribution in the cupric-silver stained reconstructed rat brains demonstrated a leftward shift toward the darker shades, indicating increased staining in the exposure groups compared to the clean control group (Figs. 3 through 5).

Table 1 shows the brain and debris field volumes for each of the groups. Debris field volume in the repeat exposure group was significantly ($p < 0.05$) greater than in the clean control, acute, or trigger groups. While lesion volume in both

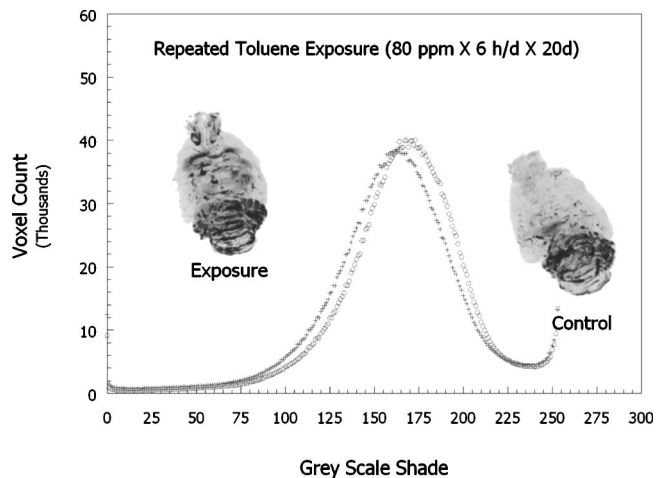


Fig. 3 Voxel distribution of Cu-Ag stain in the repeat exposure group (crosses) and the clean control group (open circles).

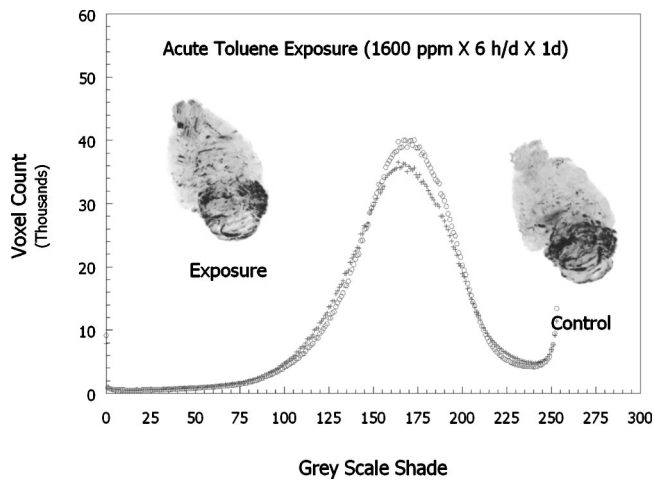


Fig. 4 Voxel distribution of Cu-Ag stain in the acute exposure group (crosses) and the clean control group (open circles).

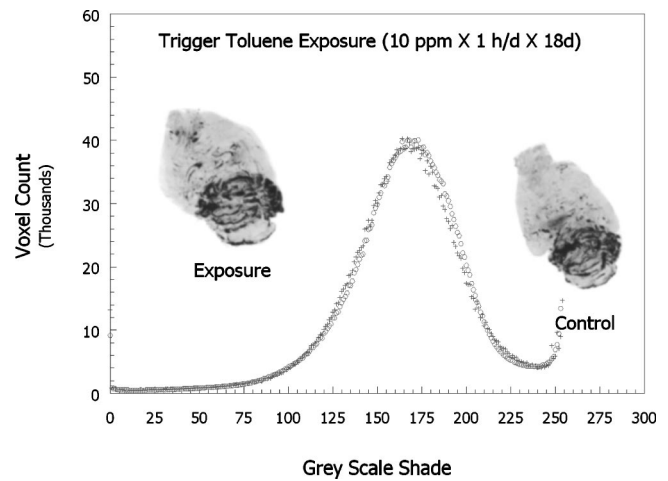


Fig. 5 Voxel distribution of Cu-Ag stain in the trigger exposure group (crosses) and the clean control group (open circles).

acute and trigger groups were greater than in the clean control group, the difference was not statistically significant. Total brain volume for each of the groups was also not statistically different.

4 Discussion

A resolution of 600 dpi (42.3 $\mu\text{m}/\text{pixel}$) in the gray-scale reflective scanning mode produced images of acceptable resolution for visualizing stained cellular debris. The choice of 600 dpi was the result of an attempt to balance resolution versus computing power requirements. Attempts to use higher resolutions generated larger files, which resulted in significant increases in processing time for the 400-MHz CPU computer used in the analysis. Current 2.5-GHz CPU technology and flat bed scanners that have optical resolutions as high as 6400 dpi (4 $\mu\text{m}/\text{pixel}$) can be obtained for much the same price as was paid for the equipment that was used in this study. A 10-fold increase in resolution is now easily possible with current desktop technology.

Since the right and left halves of the coronal sections are mirror images, Photoshop™ reasonably accurately centers the sections laterally. However, because the sections are not symmetrical about the horizontal axis, a small amount of shear effect in the dorsolateral direction was observed. While no attempt was made to correct this shear effect in this study, dorsoventral alignment can be achieved by resizing the canvas

to that presented in a standard stereotactic atlas, identifying the appropriate coronal section, choosing two anatomical structures, and translating the image to the specified coordinates. While the process is easy and can produce reasonably good results, it is time consuming. Alternatively, the align function in the VoxBlast suite will also work well, but is likewise time consuming. Alignment software “sEM Align” available for free download from Synapse Web is easy to use and enables overlay alignment. For sets of serial sections where reference rods are imbedded into the matrix, manual alignment is very accurate and fast, particularly with the “sEM” Align utility.

An automated alignment process is certainly desirable. On the other hand, if the investigator has only a relatively small data set of this type or analysis is done infrequently, justifying the cost of an automated system of alignment may be difficult. Several software products that enable automated alignment are commercially available. These packages are very expensive and may not represent an efficient use of time since setup may require as much time as processing the images by hand.

Additional distortion of the rendered image can result from the sectioning process. Sections that deviate from the true coronal plane can result from inaccurate positioning of the brains in the cutting block. The proprietary MultiBrain™ imbedding system utilized by NeuroScience Associates uses anatomical features to accurately position the brains in the imbedding medium, thereby minimizing coronal distortion and misalignment relative to the other tissue in the block. In general, sections cut from tissue embedded in paraffin will be compressed during the initial phase of the cutting and stretched during the latter portion of the cut. The brains from this study were embedded in a gelatin matrix, which has an elastic memory. Compression and stretch distortion are minimized due to elastic return of the gelatin matrix to its original shape after the cut. In addition to section alignment, sEM Align can also apply a variety of affine transformations to the section images to correct distortions. In addition to accurate specimen positioning, the MultiBrain™ technology ensures uniform section thickness. Uniformity in section thickness is critical to maintaining consistency in scanned image intensity.

Table 1 Brain and neuronal debris field volumes.

Group	Brain Volume cc ³	Neuronal Debris Field Volume cc ³
Clean	1.89±0.26	0.21±0.06
Repeat	1.89±0.13	0.28±0.07*
Acute	1.83±0.13	0.24±0.06
Trigger	1.85±0.14	0.22±0.08

* $p > 0.05$ vs. Clean.

While the spatial and temporal uniformity of the scanner were not tested, the intensities of the scanned images in this study appeared to be uniform and consistent with the original stained slides. However, in situations where uneven illumination due to thickness nonuniformities results in significant variations in intensity, dynamic thresholding can potentially compensate without degrading high-frequency details such as edge definitions and may bring out details that have been obscured by static thresholding.

While several 3-D reconstruction software packages are commercially available, VoxBlast™ was chosen for its ease of use, broad platform application, transparency control/rendering features, and reasonable cost. The palette editor in VoxBlast provides a high degree of control over the opacity and color of the rendered image, enabling an infinite range of transfer functions to be applied to the image reconstruction. The resulting reconstruction can be easily adjusted to emphasize specific pathology or regions of interest. While the maximum intensity mode may not be the best for depicting anatomic detail, it was sufficient to delineate the debris fields' anatomical distribution. The use of structure- or pathology-specific stains increases contrast significantly, enabling the voxel analysis features of VoxBlast™ to identify, quantify, and extract regions of interest. Rendering the 73 image data sets that were generated in Photoshop™ required approximately 30 s, and represented the most significant computer load of the analysis method.

Following toluene exposure and a 16-day "rest" period, the rodents used in this study were subjected to 4 weeks of operant testing prior to euthanasia and histological preparation of their brains. The resultant neuronal degeneration as defined by the cupric silver stain was primarily residual neuronal cellular and axonal debris. The locations and distribution of the debris fields, nevertheless, provided a generalized indication of the extent of the injuries and their localization. More importantly, the volume of the debris fields could be estimated and subjected to statistical analysis from which inferences could be drawn relating the exposure scenario, operant performance, and level of injury.

In a recently published study, Rodgers et al.⁶ described operant task learning decrements in rats exposed to the toluene scenarios described here. Their findings suggest a significant increase in task performance time for repeat and acute exposure groups as compared to a clean air control. In addition, all rodents exposed to toluene regardless of the exposure scenario required a statistically greater number of responses to obtain a reward during operant testing.⁶ These observations are consistent with the findings of this study in that repeated low-level exposure group demonstrated a statistically larger neuronal debris volume in regions of the brain known to be either directly or indirectly involved with memory, learning, or cognition. Both the acute and trigger groups also had larger neuronal debris volumes than the clean air control, although they were not statistically greater. While failure to detect differences between the acute, trigger, and control groups could be explained by the insensitivity of the method, alternatively, this may be a consequence of insufficient statistical power for discriminating between the subtle volume differences due to the small sample population available to this study.

A new technique referred to as voxel-based lesion-symptom mapping (VLSM) was recently described by Bates

et al. for correlating tissue damage and functional impairment.⁷ In this method, patient groupings are established based on specific behavioral and cognitive deficits. Neuroimages such as those obtained from positron emission tomography (PET) or functional magnetic resonance imaging (fMRI) are reconstructed in a common stereotactic space then compared to images from patients with no deficits. Image subtraction can reveal regions of the brain that appear to be associated with the specific impairments. The regions can then be quantified by voxel analysis. The method that is demonstrated in this paper enables similar analytical capabilities in experimental laboratory animal preparations. However, since several specific structural stains can be applied to tissue sections obtained from experimental animals, significantly greater precision and more detailed information could potentially be realized in the localization of function and relation to structure.

Silver degeneration methods are most definitive when applied to brain tissue sections from animals sacrificed 2 to 3 days after injury.^{8,9} Disintegration of neural elements has already begun by this time. Survival times of 2 and 7 days as well as 2, 4, and 8 weeks are often used so that acute effects (2 and 7 days), and delayed effects (2, 4, and 8 weeks) can be depicted.¹⁰ If, as in this study, operant testing requires a fixed survival time (i.e., 4 weeks) the persistence of axonal debris can still enable damage to be detected. Residual cell body debris may still be present and may persist as long as 9 months after the insult.¹⁰

Analysis of individual histological slices can be extremely time consuming, particularly when attempting to estimate the extent and distribution of tissue degeneration in a large sample population. In lieu of the 3-D analysis, a series of individual histograms could have been generated for each of the 2-D sections. In this study, 32 brains were cut into 73 coronal sections, yielding 2336 images. While the process is straightforward, the time required to generate histograms, isolate the specific pixel shades of interest, then do the volumetric calculations for this many slices would be prohibitive. Automation of the process, while possible, would require additional software, potentially increasing the cost of the analysis substantially.

For experienced pathologists and investigators who routinely work with serial tissue sections, developing a 3-D mental image of the distribution of a specific pathology poses little difficulty. For investigators who only occasionally work with serial tissue sections, 3-D rendering can be an effective way of representing large volumes of anatomical data. Three-dimensional visualization offers the particular advantage of being able to rapidly visualize and establish relationships between specific structures of interest and surrounding tissue anatomy that may not be perceived in 2-D images. Three-dimensional reconstruction enables convenient measurement of distances between areas of interest as well as enabling rapid volume measurements. Additionally, 3-D reconstructive modeling of tissue can facilitate generation of multiple views, cutaway views, and detailed views of tissue structures, and facilitates the same options for region/regions of interest. In experiments where degenerative processes are being studied, 3-D renderings at regular time intervals enable the degenerative process to be animated. As 3-D imaging techniques improve, broader insights will be gained into the spatial distri-

bution of tissue degenerative processes, as well as the relationships between tissue structure and function.¹¹

References

1. L. Antiga, B. Ene-Iordache, G. Remuzzi, and A. Remuzzi, "Automatic generation of glomerular capillary topographical organization," *Microvasc. Res.* **62**, 346–354 (2001).
2. E. Aratacho-Perula, R. Roldan-Villalobos, and L. Cruz-Orive, "Application of the fractionator and vertical slices to estimate total capillary length in skeletal muscle," *J. Anat.* **195**, 429–473 (1999).
3. M. Furusato, S. Wakui, M. Suzuki, K. Takagi, H. Msao, M. Asari, Y. Kano, and S. Ushigome, "Three-dimensional ultrastructural distribution of cytoplasmic interdigitation between endothelium and pericyte of capillary in human granulation tissue by serial reconstruction method," *J. Electron Microsc.* **39**, 86–91 (1990).
4. E. M. Brey, T. W. King, C. Johnston, L. V. McIntire, G. P. Reece, and C. W. Patrick, "A technique for qualitative three-dimensional analysis of microvasculature structure," *Microvasc. Res.* **63**, 279–294 (2002).
5. J. S. de Olmos, C. A. Beltramino, and S. de Olmos de Lorenzo, "Use of an amino-cupric-silver technique for the detection of early and semiacute neuronal degeneration caused by neurotoxicants, hypoxia, and physical trauma," *Neurotoxicol. Teratol.* **16**(6), 545–561 (1994).
6. W. R. Rogers, C. S. Miller, and L. Bunegin, "A rat model of neurobehavioral sensitization to toluene," *Toxicol. Ind. Health* **15**, 356–369 (1999).
7. E. Bates, M. Wilson, A. P. Saygin, F. Dick, M. I. Serno, R. T. Knight, and N. F. Dronkers, "Voxel-based lesion-symptom mapping," *Nat. Neurosci.* **6**(5), 448–450 (2003).
8. T. L. Butler, C. A. Kassed, P. R. Sanberg, A. E. Willing, and K. R. Pennypacker, "Neurodegeneration in the rat hippocampus and striatum after middle cerebral artery occlusion," *Brain Res.* **929**(2), 252–260 (2002).
9. S. Haga, C. Haga, T. Aizawa, and K. Ikeda, "Neuronal degeneration and glial cell-responses following trimethyltin intoxication in the rat," *Acta Neuropathol. (Berl)* **103**(6), 575–582 (2002).
10. K. Rupalla, P. R. Allegrini, D. Sauer, and C. Wiessner, "Time course of microglia activation and apoptosis in various brain regions after permanent focal cerebral ischemia in mice," *Acta Neuropathol. (Berl)* **96**(2), 172–178 (1998).
11. A. W. Toga and T. L. Arnica-Sulze, "Digital image reconstruction for the study of brain structure and function," *J. Neurosci. Methods* **20**, 7–21 (1987).